Fast 3D image reconstruction for rotating slat collimated gamma cameras

Roel Van Holen, Stefaan Vandenberghe, Steven Staelens, Yves D'Asseler and Ignace Lemahieu

***Abstract*—As an alternative to the use of traditional parallel hole collimators, SPECT imaging can be performed using rotating slat collimators. A gain in image quality could be expected from the higher photon collection efficiency, however, the plane integral data measured by this type of collimator require a reconstruction to invert the three-dimensional (3D) Radon transform. The use of iterative methods to do fully 3D reconstruction is computationally much more expensive compared to a classical SPECT reconstruction. A computationally attractive alternative to direct 3D reconstruction could be to use two subsequent inversion steps, where the first step would consist of reconstructing the plane integral data to conventional SPECT sinograms and the second step would be a classical SPECT reconstruction. In this work, an algorithm of the Maximum Likelihood Expectation Maximization (MLEM) type which integrates these two steps into one algorithm is proposed as an alternative to two subsequent MLEM reconstructions. A simulation study validates the new approach with respect to a two step MLEM reconstruction. Results indicate that the integration of two MLEM iteration loops into one can provide improved image quality regarding contrast recovery and noise. Moreover it avoids determining a stopping rule for the first step in the 2-step approach.**

***Index Terms*—SPECT, image reconstruction.**

I. Introduction

IN SPECT imaging, image quality is limited by the intrinsic spatial resolution versus sensitivity trade-off resulting from the geometric properties of parallel hole collimators, which are traditionally used to obtain photons from the direction perpendicular to the collimator. While maintaining the same Field Of View (FOV), rotating slat collimators (RSC) provide a better spatial resolution versus sensitivity compromise. This is due to the much higher photon collection efficiency of the plane integrals, measured by this device. Therefore, RSC can potentially provide a gain in image quality.

The collection of plane integrals of a 3D activity distribution by spinning the detector around its own axis at each regular SPECT angle can be seen as the 3D Radon transform when ignoring the effects of attenuation, depth dependent blurring and depth dependent sensitivity. For image reconstruction, a 3D algorithm which inverts the 3D Radon transform is mandatory. A Filtered Back-Projection (FBP) implementation of this 3D Radon inversion has been previously developed by Lodge [1] and by Zeng [2], an iterative RBI-EM approach has been proposed by Wang [3]. The iterative approach offers better noise characteristics, since it models the Poisson statistics of the data while it can also incorporate the effects of depth dependent blur and sensitivity into the system matrix. A drawback of the iterative approach is that it is computationally very expensive which makes it less attractive for practical use. A computationally less demanding alternative to the 3D Radon inversion is a 2-step algorithm which first reconstructs the plane integral data to conventional sinograms before reconstructing the 3D object from these sinograms using a classical SPECT reconstruction. This approach has been proved to be feasible [4], but is less accurate than a fully 3D reconstruction. In this work we propose a new technique for reconstructing plane integral data based on an integrated iterative reconstruction algorithm. The newly developed method differs from the 2-step approach in the sense that both, previously separate iteration loops, are now integrated in 1 iteration loop as illustrated in Fig. 1. First, the current image estimate is forward projected to sinogram data, which are then forward projected to plane integral data. Next, the ratio of the measured plane integral data and the forward projected plane integral data is back projected to sinogram space. At this point, a back projection to 3D image space is performed, yielding the next image estimate.

We performed a simulation study to obtain contrast to noise properties of both a 2-step MLEM (2S-MLEM) reconstruction and the newly developed Integrated MLEM (I-MLEM). The computation time will be discussed and compared to a fully 3D algorithm.

R. Van Holen, S. Vandenberghe, S. Staelens, Y. D'Asseler and I. Lemahieu are with the Department of Electronics and Information Systems, Ghent University, B-9000 Ghent, Belgium e-mail: (Roel.VanHolen@UGent.be).

This work was supported in part by the Institute for the Promotion of Innovation by Science and Technology, Flanders, IWT, Belgium.

II. Methods

A. Phantom simulation

The data used in this study were generated using a Monte Carlo simulations. Once the origin and direction of a photon was calculated using Monte Carlo techniques, the photon was further tracked geometrically. Both the detector and the collimator were modeled to be a perfect absorber. Thus, every photon striking the collimator was discarded while every photon arriving at the detector was detected. No attenuation or scatter was modeled, but the data are Poisson distributed. The plane integral data were simulated to contain a total of 50 million events. A numerical image quality phantom was simulated and consisted of a warm cylinder (diameter: 180 mm, height 216 mm), containing 4 hot spheres (diameters: 5.4 mm, 9 mm, 12.6 mm, 16.2 mm) and two cold spheres (diameters:19.8 mm and 23.4 mm). The sphere-to-background activity ratio was set 8:1 for the hot spots. In the simulation, the detector rotated around the phantom in 120 discrete angles, equally spread over 360°. At each of these SPECT angles,

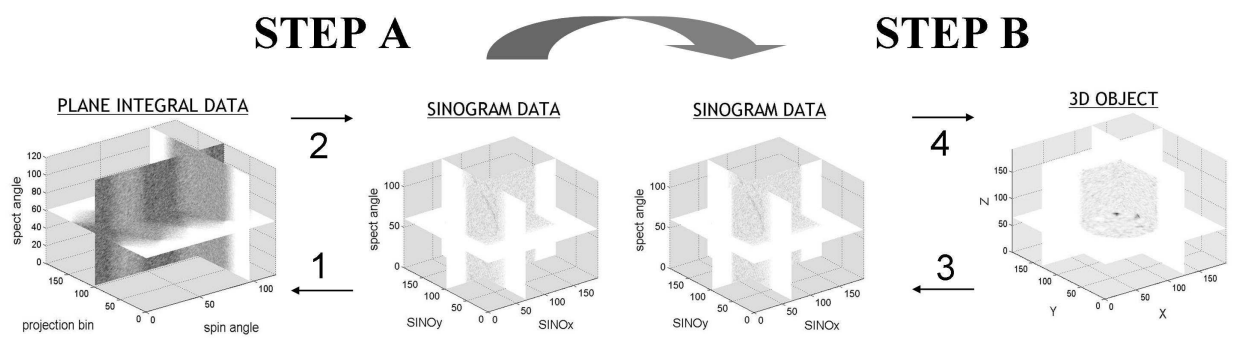

(a)

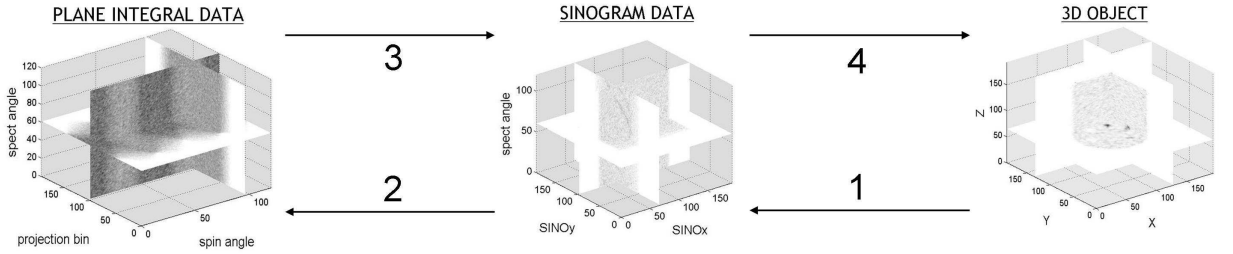

(b)

Fig. 1. In the 2S-MLEM reconstruction (a), sequence 1-2 (step A) is the first MLEM algorithm which reconstructs the sinogram data. Once the sinogram data are reconstructed, the second MLEM algorithm is performed by iterating loop 3-4 (step B). This yields the final 3D image. In the I-MLEM algorithm (b), 1 iteration involves sequence 1-2-3-4.

the detector rotated around its own axis in 120 discrete spin angles, again equally spread over 360°. The detector itself consisted of 192 by 192 detection elements, each measuring 1.8 mm by 1.8 mm. Parallel to the detector elements in one direction, a slat with finite width of 0.3 mm was simulated in between every two neighboring detector pixel rows. The height of the slats was set to 40 mm, while their length was equal to the length of the detector, being 345.6 mm. This collimator configuration results in a collimator spatial resolution of about 5 mm at 10 cm collimator distance. The SPECT rotation radius of the detector was 18 cm.

B. Image reconstruction

We used 2 different image reconstruction algorithms based on the Maximum Likelihood Expectation Maximization (MLEM) algorithm, namely the 2S-MLEM and the I-MLEM algorithm. These reconstruction methods are illustrated in Fig. 1. The reason for choosing MLEM is to avoid interference of any extra reconstruction parameters (such as the number of subsets when using OSEM).

1) 2S-MLEM: The first step of the algorithm (step A) involves a calculation of the sinogram data, independently for every fixed SPECT angle θ using MLEM:

$$s_i^{t+1} = \frac{s_i^t}{\sum_j A_{ij}} \sum_j A_{ij} \frac{g_j}{\bar{g}_j^t}, \quad (1)$$

with

$$\bar{g}_j^t = \sum_n A_{nj} s_n^t, \quad (2)$$

and where s_i^t is the estimate at iteration t of the sinogram data at bin i, g_j are the observed plane integral data at projection bin j and A_{ij} is the system matrix that models the step to go from sinogram data to plane integral data. We want every SPECT angle to be treated separately, so A_{ij} is zero if i and j do not correspond to the same SPECT angle θ (i.e. $\theta_i \neq \theta_j$). In system matrix A, we do not include any sensitivity modeling. This can be justified since the sensitivity in a plane parallel to the detector is quite uniform, in contrasts to the $\cos\alpha$ dependency when a strip detector is used [4]. Moreover, the resolution which is only dependent on the source to collimator distance, will not be modeled in this step.

After performing T iterations of this first step, the obtained sinogram is used as an input for the second step. This step (step B) is analogous to the first except for the system matrix B_{ki} which includes both a model for depth dependent sensitivity and depth dependent blur. This matrix models the contribution from image voxels to sinogram elements. This is similar to a classical 3D SPECT reconstruction, except for the sensitivity modeling. The algorithm can be written as:

$$f_k^{t+1} = \frac{f_k^t}{\sum_i B_{ki}} \sum_i B_{ki} \frac{s_i^T}{\bar{s}_i^t}, \quad (3)$$

with

$$\bar{s}_i^t = \sum_n B_{ni} f_n^t, \quad (4)$$

where f_k^t is the object estimate at iteration t of voxel k, s_i^T are the sinogram data at bin i, obtained by iterating the previous step T times.
The main problem with this method is the determination of T, or in other words, to define a stopping rule for the first MLEM algorithm. If T is chosen too small, we can never reach the desired contrast in the images produced by step B. If, on the other hand, T is chosen too high, the output of step B would immediately be too noisy. In this study, the stopping rule will be derived empirically for the phantom under consideration. Step A will be stopped at different iteration points before step B reconstruction. On the resulting images, a contrast to noise analysis will point us to the optimal number T.

2) Integrated MLEM: The integration of both steps in one iteration loop results in an algorithm of the form

$$f_k^{t+1} = \frac{f_k^t}{\sum_i B_{ki}} \sum_i B_{ki} \frac{\frac{s_i^{t-1}}{\sum_j A_{ij}} \sum_j A_{ij} \frac{g_j}{\bar{g}_j^t}}{\bar{s}_i^t}, \quad (5)$$

with

$$\bar{g}_j^t = \sum_l A_{lj} \bar{s}_l^t \quad (6)$$

$$= \sum_l A_{lj} \left\{ \sum_n B_{nl} f_n^t \right\}. \quad (7)$$

The main difference with the previous method is that when integrating both iteration loops, the estimate of the sinogram data s_j at SPECT angle θ is dependent not only on g_j at that angle θ, but on the complete plane integral data. With this method, the data are kept more consistent in the sense that the all data now are used to provide information on each SPECT angle through the iteration process. In step A of the 2S-MLEM, only the data measured at SPECT angle θ provide information on SPECT angle θ of s_j.

III. Results

A. Determination of T

To determine the number of iterations for step A in the 2S-MLEM reconstruction, step A was stopped at 4 different iteration points: for T equal to 25, 50, 75 and 100. All four sinograms were reconstructed using step B. A contrast to noise analysis on the largest hot lesion in the images resulting from step B (Fig. 2) shows that for $T > 50$, the noise increases without substantially improving the contrast.

On the other hand, we can see that the contrast for $T = 25$ is limited because step A did not converge yet. Since these findings can be extrapolated to the other lesions, $T = 50$ is chosen for further comparison with the I-MLEM algorithm.

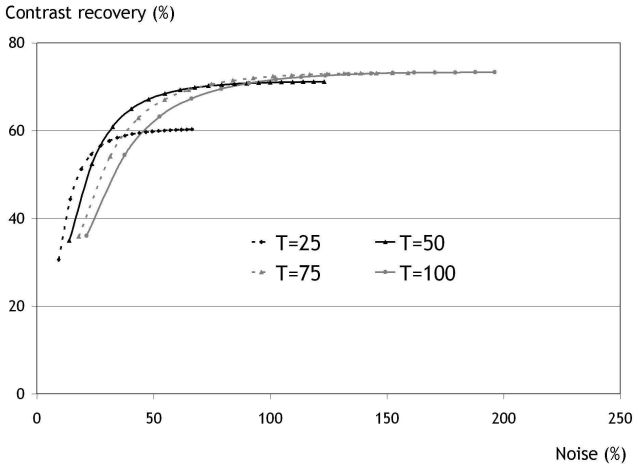

Fig. 2. Contrast to noise plot for different values of T (for 16.2 mm diameter hot lesion). It can be seen from this plot that the best contrast noise trade-off is found for $T = 50$.

B. Comparison of 2S-MLEM and I-MLEM

The 2S-MLEM (50 iterations of the first step) and I-MLEM reconstruction techniques are compared by means of contrast to noise plots for both the 16.2 mm diameter hot lesion and the 23.4 mm diameter cold lesion. Results are shown in Fig. 3 and Fig. 4 respectively. Every fifth iteration is plotted as a discrete point, starting from iteration number 5. It can be seen that for a noise level of about 40%, we need about 20 step B iterations for the 2S-MLEM while we need about 40 iterations of the I-MLEM algorithm. At this point, the hot spot and cold spot contrast reached are respectively aboutby 8% and 13% higher for the I-MLEM compared to 2S-MLEM. Similar improvements were found for the other lesion sizes. In Fig. 5, transversal slices through the reconstructed images are shown together with a central profiles. The noise in both images was matched at 40%. The slight increase in contrast recovery appears as a lower background activity in the I-MLEM slice. The profile show that especially for the cold lesion, the contrast is better for the integrated reconstruction method.

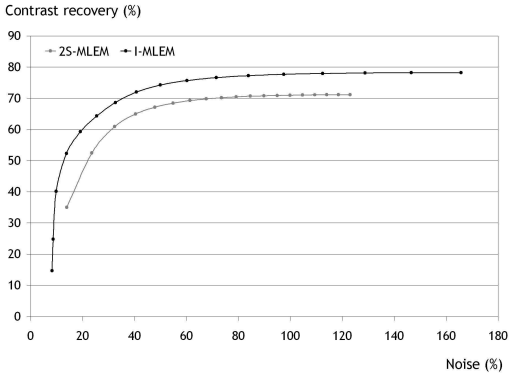

Fig. 3. Contrast noise plot for 16.2 mm diameter hot lesion. The contrast reached by the I-MLEM is about 8% higher than the contrast reached by the 2S-MLEM method.

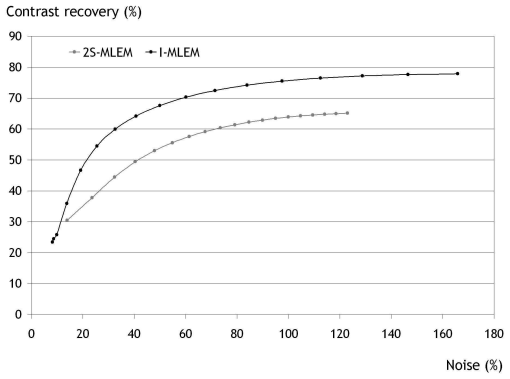

Fig. 4. Contrast noise plot for for 23.4 mm diameter cold lesion. The contrast improves with about 13% for the integrated method.

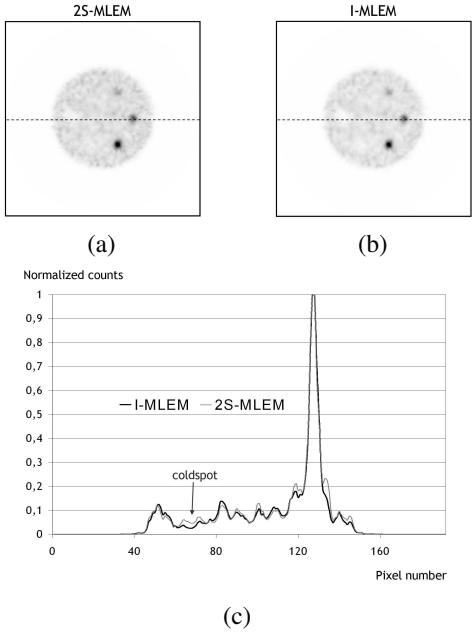

Fig. 5. (a) and (b) respectively show a transversal slice through the 2S-MLEM reconstructed image and through the I-MLEM reconstructed image. Profiles profile drawn across the central horizontal line are shown in (c).

C. Computation time

The computation time required for one iteration of I-MLEM is about 18 minutes. This is equal to the time required for one iteration of both steps in 2S-MLEM (Fig. 6). The reason for this is that both algorithms use the same projector/back projector pairs. For comparison, the reconstruction time for one iteration of our fully 3D MLEM algorithm is also plotted. It can be seen that the speed up by using a two step algorithm instead of a real 3D algorithm reduces the computation time with two orders of magnitude.

IV. Discussion

Reconstructing plane integral data based on a 2-step approach is a computationally attractive alternative to fully 3D reconstruction. The problems concerning the stopping rule of the first step when using iterative reconstruction methods however limit the flexibility of this approach since this parameter is object and activity dependent. The integration of both MLEM loops, replacing the two separate reconstructions, cancels out this problem. Furthermore, due to the data that are kept more consistent, an improved contrast versus noise balance could be obtained by integrating both steps. Since matrix B_{ki} includes both sensitivity and resolution modeling, the computation time of the projections and back projections associated with it will be dominating the computation time. Therefore, for the phantom used in this study, where we need more iterations of the I-MLEM than for the 2S-MLEM reconstruction, the I-MLEM will take more computation time (about the double) than the 2S-MLEM method. However, looking at the huge gain in speed compared to a fully 3D algorithm, this increase in computation time for I-MLEM is small.

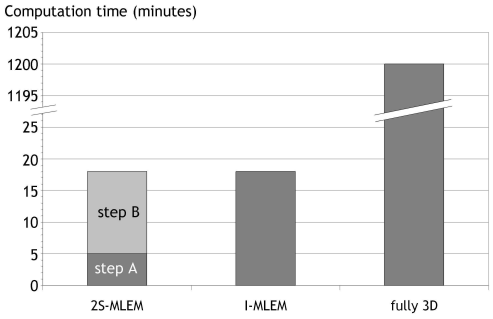

Fig. 6. The computation time for one iteration of 2S-MLEM and I-MLEM is shown together with the time required for one fully 3D iteration.

V. Conclusion

In this paper we show that a 2-step MLEM algorithm can be successfully replaced by an algorithm which integrates both MLEM reconstructions. Not only did we see an increase in image quality arising from the integration, we also avoided the problems concerning the stopping rule for the first step in a 2-step MLEM approach. The reduction of the computational burden associated with a fully 3D MLEM reconstruction, which was the motivation for this work, seemed to be successful. A reduction in computation time by two orders of magnitude could be obtained. Future work will show how the image quality of I-MLEM compares to that of fully 3D MLEM.

References

[1] M.A. Lodge, S. Webb, M.A. Flower, en D.M. Binnie, "A prototype rotating slat collimator for single photon emission computed tomography," *IEEE Transactions on Medical Imaging*, vol. 15, no. 4, pp. 500–511, 1996.

[2] G. L. Zeng, D. Gagnon, C. Matthews, J. Kolthammer, J. Radachy, en W. Hawkins, "Image reconstruction algorithm for a rotating slat collimator," *Medical Physics*, vol. 29, no. 7, pp. 1406–1412, 2002.

[3] W. Wang, W. Hawkins, en D. Gagnon, "3D RBI-EM reconstruction with spherically-symmetric basis function for SPECT rotating slat collimator," *Physics in Medicine and Biology*, vol. 49, no. 11, pp. 2273–2292, 2004.

[4] G. L. Zeng, "Detector blurring and detector sensitivity compensation for a spinning slat collimator," *IEEE Transactions on Nuclear Science*, vol. 53, no. 5, pp. 2628–2634, 2006.